Haptotropic Rearrangements in Sandwich (Fluorenyl)(Cyclopentadienyl) Iron and Ruthenium Complexes

Evgueni Kirillov, Samia Kahlal, Thierry Roisnel, Thomas Georgelin, Jean-Yves Saillard,* and Jean-François Carpentier*

UMR 6226 Sciences Chimiques de Rennes, CNRS-University of Rennes 1, 35042 Rennes Cedex, France

Received November 3, 2007

Haptotropic rearrangements in sandwich (Cp)M(η^n-Flu) (M = Fe, Ru; Flu = fluorenyl) complexes were investigated by theoretical (DFT) methods and experimental techniques as well in the iron case. The molecular structure of the (Cp)Fe(η^5-Flu) isomer (**A-Fe**) was determined by an X-ray diffraction study. The activation barrier for the η^6-Flu (**B-Fe**, kinetic product) $\leftrightarrows$ η^5-Flu (**A-Fe**, thermodynamic product) process in the iron complex was determined by ^{1}H NMR to be 31.4 ± 2.2 kcal·mol^{-1} in benzene. Using DFT calculations for the $\eta^6 \leftrightarrows \eta^5$ process in (Cp)M(η^n-Flu) (M = Fe, Ru), two stable intermediates were found, i.e., η^3-"frontside" (**C**) and η^4-"backside" (**D**) species. The "frontside" pathway was found to be 4–5 kcal·mol^{-1} more favorable than the "backside" pathway for both the Fe and Ru complexes. The corresponding activation barriers were found to be 27.3 (B3LYP set) and 33.2 (BP86 set) kcal·mol^{-1} for the Fe complexes and 27.9 kcal·mol^{-1} (B3LYP set) for the Ru complexes.

Introduction

Haptotropic rearrangement reactions (HRR) in transition metal complexes containing polyenic ligands have been considerably studied, both experimentally and theoretically, over the past 30 years.[1–3] These unique migration reactions are often associated with low activation barriers and can be easily followed by spectroscopic techniques at reasonable temperatures. We have been recently involved in the use of the fluorenyl ligand ($C_{13}H_9^-$, Flu^-) for designing early transition metal complexes that are of significant interest in polymerization catalysis.[4] From this point of view, the coordination mode (hapticity) of the fluorenyl ligand is of crucial interest.[1]

Scheme 1

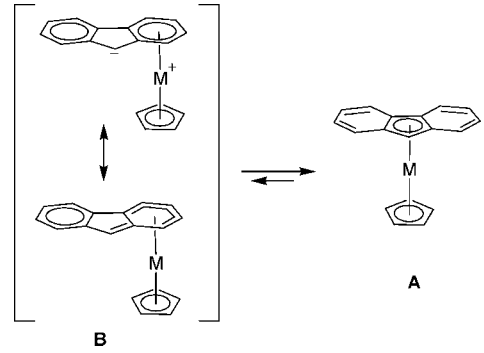

In this paper, we report our experimental and theoretical investigations on the dynamics associated with changes in the fluorenyl coordination mode in (Cp)M(η^n-Flu) (M = Fe, Ru) complexes. The Flu^- ligand offers to the M(II) d^6 metal center two different sites of coordination for which the 18-electron rule is satisfied. One corresponds to the η^5 coordination of the central C_5 ring (structure **A** in Scheme 1) and the other one to the (somewhat distorted, see below) η^6 coordination of one of the C_6 rings (structure **B** in Scheme 1). A type **B** structure has been determined for (Cp)Fe(η^6-Flu) in the solid state.[5] It exhibits a long Fe−C(10) bond, indicating a distortion toward η^5 corresponding to one of the Lewis formulas depicted in Scheme 1 for **B-Fe**. On the other hand, a type **A** structure was found for (C_5Me_5)Ru(η^5-Flu), also by X-ray diffraction studies.[6] The **B-Fe** $\leftrightarrows$ **A-Fe** HRR for the iron complex has been reinvestigated by Novikova et al.[2] The reaction was monitored by electronic spectroscopy in xylene solution, and an activation barrier of 22.5 kcal·mol^{-1} was determined.

We report herein (i) the characterization and crystal structure of **A-Fe** ((Cp)Fe(η^5-Flu)), (ii) the reinvestigation of the **B-Fe**

* Corresponding authors. E-mail: jean-yves.saillard@univ-rennes1.fr; jcarpent@univ-rennes1.fr.

(1) (a) Selected references on HRR mechanisms: Ahn, N. T.; Elian, M.; Hoffmann, R. *J. Am. Chem. Soc.* **1978**, *100*, 110. (b) Oprunenko, Yu., F. *Russ. Chem. Rev.* **2000**, *69*, 683. (c) Oprunenko, Yu. F.; Akhmedov, N. G.; Laikov, D. N.; Malyugina, S. G.; Mstislavsky, V. I.; Roznyatovsky, V. A.; Ustynyuk, Yu. A.; Ustyniuk, N. A. *J. Organomet. Chem.* **1999**, *583*, 136. (d) Trifinova, O. I.; Ochertyanova, E. A.; Akhmedov, N. G.; Roznyatovsky, V. A.; Laikov, N. A.; Ustynyuk, Yu. A.; Ustynyuk, N. A. *Inorg. Chim. Acta* **1998**, *280*, 328. (e) Pomazanova, N. A.; Novikova, L. N.; Ustynyuk, N. A.; Kravtzov, D. N. *Metalloorg. Khim.* **1989**, *2*, 422. (f) Calhorda, M. J.; Veiros, L. F. *Comments Inorg. Chem.* **2001**, *22*, 375. (g) Calhorda, M. J.; Goncalves, I. S.; Goodfellow, B. J.; Herdtweck, E.; Romao, C. C.; Royo, B.; Veiros, L. F. *New J. Chem.* **2002**, *26*, 1552. (h) Veiros, L. F. *Organometallics* **2006**, *25*, 2266. (i) Romão, C. C.; Veiros, L. F. *Organometallics* **2007**, *26*, 1777. (j) Decken, A.; Britten, J. F.; McGlinchey, M. J. *J. Am. Chem. Soc.* **1993**, *115*, 7275. (k) McGlinchey, M. J. *Can. J. Chem.* **2000**, *79*, 1295. (l) Brydges, S.; Reginato, N.; Cuffe, L. P.; Seward, C. M.; McGlinchey, M. J. *C. R. Chim.* **2005**, *8*, 1497. (m) Dötz, K. H.; Stendel, J. S., Jr.; Müller, S.; Nieger, M.; Ketrat, S.; Dolg, M *Organometallics* **2005**, *24*, 3219. (n) Shaw-Taberlet, J. A.; Sinbandhit, S.; Roisnel, T.; Hamon, J.-R.; Lapinte, C. *Organometallics* **2006**, *25*, 5311. (o) Ketrat, S.; Müller, S.; Dolg, M. *J. Phys. Chem.* **2007**, *111*, 6094. (p) Berg, D. J.; Sun, J.; Twamley, B. *Chem. Comm.* **2006**, 4119.

(2) Novikova, L. N.; Mazurchik, B. A.; Oprunenko, Yu. F.; Ustynyuk, N. A., *Russ. Chem. Bull. Int. Ed.* **2001**, *50*, 157.

(3) Albright, T. A.; Hofmann, P.; Hoffmann, R.; Lillya, C. P.; Dobosh, P. A. *J. Am. Chem. Soc.* **1983**, *105*, 3396.

(4) (a) Kirillov, E.; Toupet, L.; Lehmann, C. W.; Razavi, A.; Kahlal, S.; Saillard, J.-Y.; Carpentier, J.-F. *Organometallics* **2003**, *22*, 4038. (b) Kirillov, E.; Lehmann, C. W.; Razavi, A.; Carpentier, J.-F. *J. Am. Chem. Soc.* **2004**, *126*, 12240. (c) Kirillov, E.; Dash, A. K.; Rodrigues, A.-S.; Carpentier, J.-F. *C. R. Chim.* **2006**, *9*, 1151. (d) Rodrigues, A.-S.; Kirillov, E.; Lehmann, C. W.; Roisnel, T.; Vuillemin, B.; Razavi, A.; Carpentier, J.-F. *Chem.−Eur. J.* **2007**, *13*, 5548.

(5) Johnson, J. W.; Treichel, P. M. *J. Am. Chem. Soc.* **1977**, *99*, 1427.

(6) Gassman, P. G.; Winter, C. H. *J. Am. Chem. Soc.* **1988**, *110*, 6130.

10.1021/om701109z CCC: $40.75
Publication on Web 01/12/2008

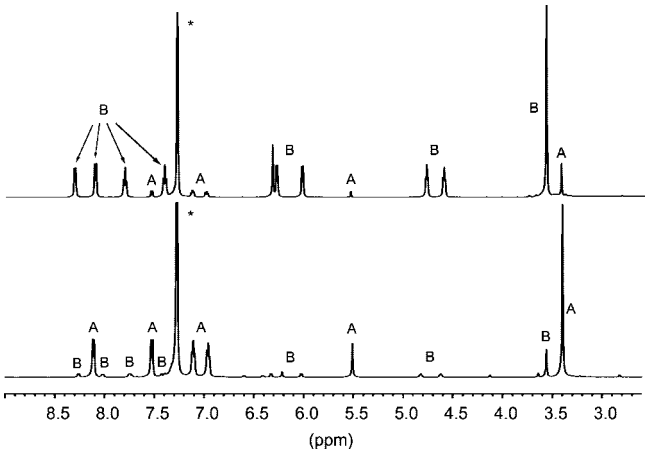

Figure 1. ^{1}H NMR spectra (500 MHz, benzene-d_6, 298 K) of the **B** ⇆ **A** HRR for (Cp)Fe(η^n-Flu): (top) initial material, i.e., ca. 6:94 mixture of (Cp)Fe(η^5-Flu) and (Cp)Fe(η^6-Flu); (bottom) product of the reaction carried out at 60 °C over 3 h, i.e., ca. 86:14 mixture of (Cp)Fe(η^5-Flu) and (Cp)Fe(η^6-Flu) (* stands for residual resonances of benzene).

⇆ **A-Fe** equilibrium by NMR spectroscopy, and (iii) a complete theoretical investigation of the possible associated HRR pathways at the DFT level. For the sake of comparison, a parallel computational study was conducted on (Cp)Ru(η^n-Flu) to explore the **B-Ru** ⇆ **A-Ru** HRR.

Results and Discussion

Spectroscopic Investigations on Haptotropic Rearrangements in (Cp)Fe(η^n-Flu). Following the reported procedure,[5] the deep green complex (Cp)Fe(η^6-Flu) (**B-Fe**) was obtained by reaction of [(Cp)Fe(η^6-fluorene)][PF_6] with potassium *tert*-butoxide in toluene at room temperature. The nature of this material was confirmed by ^{1}H NMR spectroscopy, which features predominantly a set of resonances consistent with an asymmetric type **B** structure (Figure 1, top). However, even though we carried out this deprotonation reaction strictly under the reported mild conditions, the concomitant formation of (Cp)Fe(η^5-Flu) (**A-Fe**) was found to take place systematically with ca. 6% NMR yield.[7] The latter isomer shows ^{1}H NMR resonances characteristic of its C_s symmetric structure (Figure 1, bottom).

We aimed next at investigating the **B-Fe** ⇆ **A-Fe** HRR by means of NMR spectroscopy. Previous reports have disclaimed the utility/appropriateness of this method due to substantial concomitant decomposition of the compounds in solution at 80−90 °C.[1e] In our hands, no noticeable decomposition of the reagents was detected by ^{1}H NMR spectroscopy in benzene-d_6 or cyclohexane-d_{12} over the temperature range 40–80 °C.[8] Surprisingly, we observed that the **B-Fe** ⇆ **A-Fe** HRR takes place even at 40 °C in benzene-d_6 solution, though the equilibrium state was not reached after 12 h. At 80 °C the reaction proceeded very fast and the equilibrium state was attained within a few minutes. The exponential shape of the kinetic plots obtained at 50−80 °C in benzene-d_6 or cyclohexane-d_{12} and further kinetic analyses were in agreement with reversible first-order kinetics (Table 1).

(7) The side formation of isomer **A-Fe** was not reported in the original investigations at this synthetic step; see ref 5.

(8) However, the possible formation of small amounts of paramagnetic species, not detected by NMR spectroscopy, cannot be discarded.

Table 1. Kinetic Data for the B-Fe ⇆ A-Fe Isomerization Process Derived from ^{1}H NMR Spectroscopy Data (500 MHz)

	benzene-d_6		cyclohexane-d_{12}	
T (K)	k 10^{-3} (s^{-1})	K_{eq}	k 10^{-3} (s^{-1})	K_{eq}
323	2.0	3.19	n.d.	n.d.
333	3.3	3.54	6.7	4.01
338	21.0	7.00	n.d.	n.d.
343	44.4	6.23	40.6	3.97
353	93.4	8.39	n.d.	n.d.

Table 2. Crystal Data and Structure Refinement for A-Fe

empirical formula	$C_{18}H_{14}Fe$
fw	286.14
temperature	100(2) K
wavelength	0.71073 Å
cryst syst, space group	orthorhombic, *Cmc*21
unit cell dimens	a = 15.06(2) Å, α = 90°
	b = 9.6563(16) Å, β = 90°
	c = 8.8505(15) Å, γ = 90°
volume	1287.1(17) Å^3
Z	4
density	1.477 Mg/m^3
absorp coeff	1.152 mm^{-1}
F(000)	592
cryst size	0.3 × 0.05 × 0.05 mm
θ range for data collection	3.40 to 27.52°
limiting indices	$-19 \le h \le 19$, $-12 \le k \le 12$, $-11 \le l \le 11$
no. of reflns collected/unique	3930/1438 [R(int) = 0.0368]
completeness to θ = 27.52	97.9%
absorp corr	semiempirical from equivalents
max. and min. transmn	0.944 and 0.702
refinement method	full-matrix least-squares on F^2
no. of data/restraints/params	1438/1/91
goodness-of-fit on F^2	1.037
final R indices [$I > 2\sigma(I)$]	R_1 = 0.0326, wR_2 = 0.0655
R indices (all data)	R_1 = 0.0414, wR_2 = 0.0675
absolute struct param	0.03(3)
largest diff peak and hole	0.582 and −0.371 e·A^3

The activation parameters associated with the **B-Fe** ⇆ **A-Fe**, $\Delta E^{\ddagger}_{B\to A}$ of 31.4 ± 2.2 kcal·mol^{-1} and $\Delta S^{\ddagger}_{B\to A}$ of 24 ± 5 eu, were derived from the kinetic data (see Experimental Section and Supporting Information). The value of the activation barrier is larger than the one previously determined for this system in xylene solution using electronic spectroscopy ($\Delta E^{\ddagger}_{B\to A}$ = 22.5 ± 2 kcal·mol^{-1}).[2] Attempts to perform similar quantitative experiments in cyclohexane-d_{12} failed due to low solubility of the initial material in this solvent and, as a consequence, the impossibility of keeping the concentration of the material constant. Nonetheless, it is worth noting that the few rate constants k that could be determined in cyclohexane-d_{12} were found to be of the same order of magnitude as those obtained in benzene-d_6 (Table 1). The latter observation suggests that HRR in aromatic (benzene) and aliphatic (cyclohexane) hydrocarbon solvents may proceed via the same mechanism, or at least that the possible influence/contribution of the nature of the solvent on/to this present intramolecular process is negligible.

Molecular Structure of (η^5-Flu)Fe(Cp) Isomer (A-Fe). Deep red prismatic crystals of isomer **A-Fe** suitable for an X-ray diffraction study were grown from a concentrated benzene solution at room temperature. The crystal data and refinement parameters are given in Table 2. In contrast with Cp_2Fe[9] and (C_5Me_5)Ru(η^5-Flu),[6] which both feature a perfectly eclipsed orientation of the five-membered rings, **A-Fe** adopts in the solid state a molecular structure in which the cyclopentadienyl rings

(9) (a) Seiler, P.; Dunitz, J. D. *Acta Crystallogr.* **1982**, *B38*, 1745. (b) Seiler, P.; Dunitz, J. D. *Acta Crystallogr.* **1979**, *B35*, 2020.

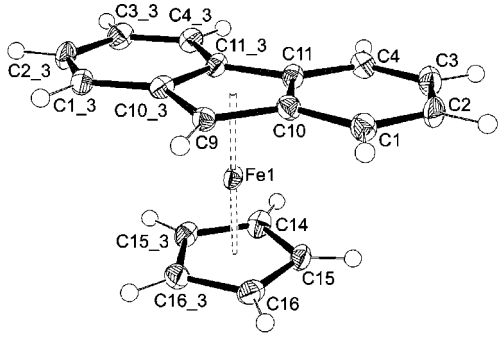

Figure 2. ORTEP structure of **A-Fe** (thermal ellipsoids at the 50% level). Selected bond lengths (Å) and angles (deg): Fe−C(9), 2.052(4); Fe−C(10), 2.100(3); Fe−C(11), 2.080(3); Fe−C(14), 2.042(4); Fe−C(15), 2.024(3); Fe−C(16), 2.040(3); Fe−Cp_{cent}, 1.635(3); Fe−Flu_{cent}, 1.681(3); Flu_{cent}−Fe−Cp_{cent}, 177.81(12).

of both Cp and Flu ligands are staggered (Figure 2). The C_s symmetry of **A-Fe** lies on a crystallographic mirror plane passing through C(9), Fe(1), and C(14) atoms. The geometry of the molecule is a typical, regular sandwich with a nearly linear Flu_{cent}−Fe−Cp_{cent} angle of 177.81(12)°. The Fe−C(Cp) distances (2.024(3)−2.042(4) Å) in **A-Fe** fall in the range of values found in isomer **B-Fe** (2.024(7)−2.048(5) Å).[5] The coordination of the fluorenyl ligand to the iron atom is clearly η^5, showing a small maximal deviation of Fe−C(Flu) distances of ca. 0.048 Å.

Theoretical Analysis. (Cp)Fe(η^n-Flu). Calculations were carried out at both the B3LYP and BP86 levels (see Computational Details). The main relevant data corresponding to the calculated stationary points (with average experimental distances given in square brackets) are given in Table 3, and their molecular structures are shown in Figure 3.

The calculated structure **A-Fe** adopts an eclipsed conformation with C_s symmetry. It should be noted that the calculated staggered conformation is almost isoenergetic (less than 0.4 kcal·mol^{-1} higher), indicating, as expected, a very low barrier for the Cp rotation. The BP86 Fe−C bond distances are slightly shorter than the B3LYP ones and are still somewhat longer than the experimental ones, as often found with DFT calculations on electron-rich transition metal complexes. Otherwise, both types of calculations lead to very similar structures with an η^5 coordination mode slightly distorted toward η^3, i.e., a metal atom somewhat shifted toward C(9). This feature is quite common in fluorenyl coordination chemistry and is related to the nature of the fluorenyl HOMO and the electron richness of C(9).[10] Structure **B-Fe** exhibits the same small differences as structure **A-Fe** with respect to the B3LYP, BP86, and experimental results. The Fe−C(Cp) distances are longer than in structure **A-Fe**. The same trend is found when comparing ferrocene to (Cp)Fe(η^6-C_6H_6)$^+$.[11] The η^6 coordination mode is distorted, with a shifting of the metal away from C(10) and with C−C distances indicating a significant weight for the η^5 limit formula of Scheme 1 (Table 3). This trend is fully consistent with the π-type electronic structure of the Flu^- ligand.[10] Both levels of calculations found **A-Fe** more stable than **B-Fe** by only a few kcal·mol^{-1}, in agreement with the fact that both isomers have been isolated and coexist at room temperature. The difference in the dipole moments of **A-Fe** and **B-Fe** suggests that the latter

Table 3. Major Computed Data for the B-Fe ⇆ A-Fe HRR Process (first values correspond to B3LYP level, values in parentheses correspond to BP86 level; values in square brackets are average experimental values for A-Fe (ref 5) and B-Fe (this work))

	A-Fe	B-Fe	C-Fe	D-Fe	TS_{A-C}	TS_{C-B}	TS_{A-D}	TS_{D-B}
HOMO–LUMO gap (eV)	3.75 (1.69)	3.04 (1.47)	3.26 (0.92)	2.25 (0.84)	2.23 (0.73)	2.45 (0.73)	2.12 (0.52)	2.34 (0.79)
rel energy (kcal·mol^{-1})	0.0 (0.0)	6.2 (2.6)	19.6 (23.2)	30.4 (28.9)	22.8 (25.8)	33.5 (35.8)	37.9 (40.9)	38.7 (40.1)
Fe−C(1) (Å)		2.218 (2.177) [2.122(5)]	2.249 (2.174)		2.389 (2.260)	2.245 (2.072)		
Fe−C(2) (Å)		2.135 (2.099) [2.053(5)]						
Fe−C(3) (Å)		2.115 (2.083) [2.039(5)]		2.384 (2.281)			2.416 (2.293)	2.153 (2.082)
Fe−C(4) (Å)		2.159 (2.118) [2.072(5)]		2.384 (2.281)				
Fe−C(5) (Å)								
Fe−C(10) (Å)	2.167 (2.134) [2.100]	2.449 (2.436) [2.316(5)]	2.129 (2.088)		2.162 (2.073)	2.105 (2.026)	2.846 (2.812)	3.030 (3.040)
Fe−C(11) (Å)	2.180 (2.144) [2.080]	2.264 (2.233) [2.175(5)]		2.144 (2.104)	3.012 (2.912)	2.433 (2.259)	2.118 (2.052)	2.161 (2.137)
Fe−C(12) (Å)	2.180 (2.144) [2.080]		3.098 (3.080)	2.144 (2.104)			2.247 (2.217)	
Fe−C(13) (Å)	2.167 (2.134) [2.100]							
Fe−C(9) (Å)	2.093 (2.065) [2.052]		2.080 (2.075)		2.098 (2.099)	2.780 (2.681)		
Fe−C(Cp) (Å) average	2.112 (2.083) [2.034]	2.125 (2.105) [2.038]	2.125 (2.080)	2.104 (2.079)	2.119 (2.073)	2.136 (2.112)	2.121 (2.069)	2.113 (2.064)
Fe−C(Cp) (Å) range	2.107–2.117 (2.077–2.089) [2.024–2.042]	2.120–2.134 (2.096–2.118) [2.030–2.048]	2.095–2.150 (2.043–2.112)	2.088–2.127 (2.058–2.113)	2.096–2.149 (2.046–2.100)	2.131–2.144 (2.085–2.137)	2.104–2.146 (2.054–2.090)	2.084–2.137 (2.021–2.092)
dipole moment μ (D)	0.18 (0.22)	4.02 (3.90)	1.79 (1.48)	2.06 (1.62)	1.71 (1.47)	2.95 (1.94)	2.68 (2.23)	2.83 (2.13)

(10) Kirillov, E.; Saillard, J.-Y.; Carpentier, J.-F. *Coord. Chem. Rev.* **2005**, *249*, 1221.

(11) Ruiz, J.; Ogliaro, F.; Saillard, J.-Y.; Halet, J.-F.; Varret, F.; Astruc, D. *J. Am. Chem. Soc.* **1998**, *120*, 11693.

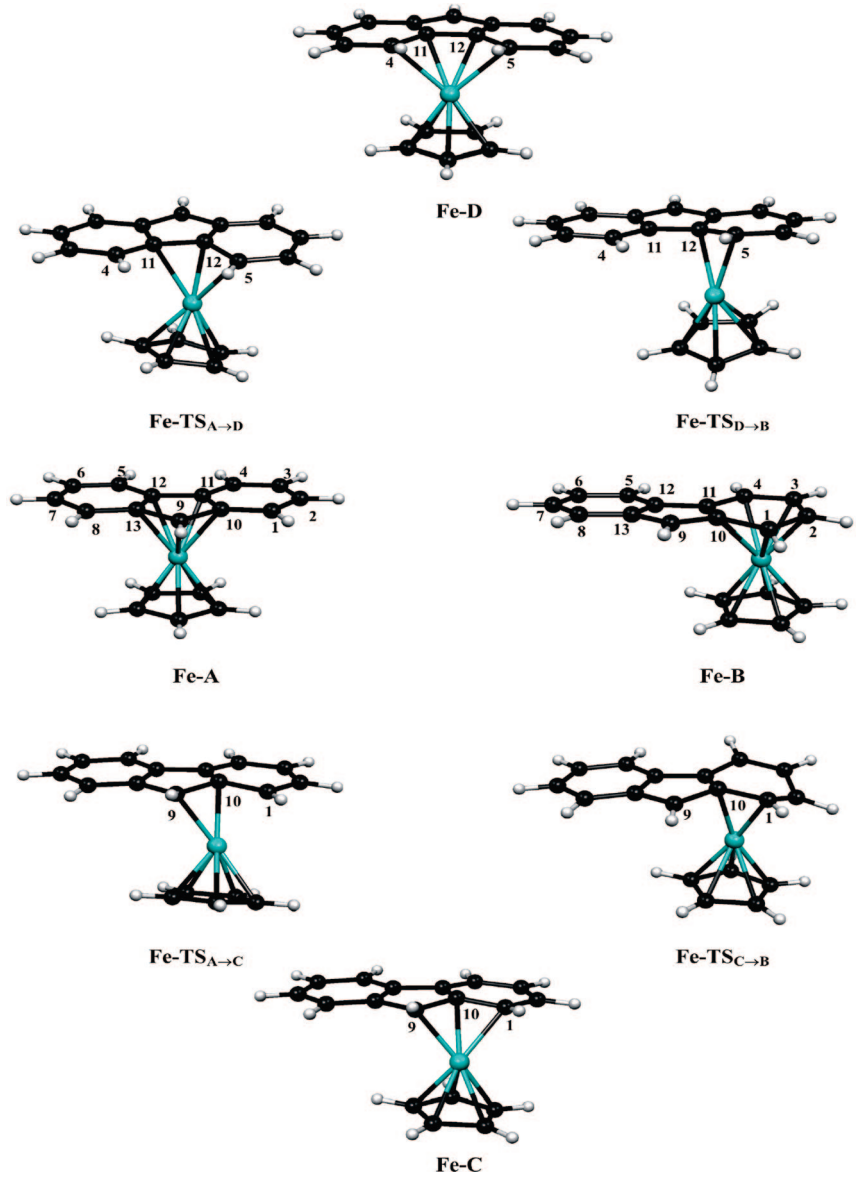

Figure 3. Optimized geometries of the various energy minima found for (Cp)Fe(η^n-Flu) and of the transition states connecting them.

structure could be the most favored in polar solvents. The MO level orderings of **A-Fe** and **B-Fe**, computed at the BP86 level, are shown in Figure 4. They exhibit the typical level ordering of iron(II) sandwich complexes,[11] with three occupied and largely nonbonding d-type levels and two vacant antibonding ones. However, a peculiar feature of **B-Fe** is the presence of a high-lying HOMO, of dominant fluorenyl character with some antibonding metal admixture (see Figure 4). In the case of **A-Fe**, this orbital is involved in the bonding with the metal and therefore mixes in levels lying at much lower energy.

In a very elegant pioneering theoretical investigation on HRR in bicyclic polyene-ML$_n$ complexes, Albright et al. found that the **A**→ **B** least-motion pathway is highly disfavored.[3] Rather, the reaction pathway is "circuitous" and should involve an intermediate in which the metal is bonded in an exocyclic way to some of the fluorenyl carbon atoms. Two possible intermediates, both η^3 coordinated and in which the metal is external to the rings, were predicted at the EHT level. The most stable involves C(9), C(10), and C(1), and the other one involves C(4), C(11), and C(12). More recent theoretical studies on related systems confirmed the non least-motion and "circuitous" nature of the pathway associated with related HRR mechanisms.[1b,c,d,l,o,p] Our exploration of the potential energy surface at the DFT level found also the least-motion pathway to be strongly disfavored. Our search for other true minima led to structures **C-Fe** and **D-Fe** (Figure 3 and Table 3). As mentioned above, the **C-Fe** structure was predicted by Albright et al. to be the more likely intermediate.[3] It exhibits an unsymmetrical η^3 coordination mode with one long (Fe−C(1)) and two short (Fe−C(9) and Fe−C(10)) bonds. A very similar exocyclic coordination mode to fluorenyl has been reported in the case of molybdenum complexes.[1g,12] Structure **D-Fe** differs somewhat from Albright's other possible intermediate. It is not a trihapto, but a symmetrical tetrahapto complex with two short (Fe−C(11) and Fe−C(12)) and two long (Fe−C(4) and Fe−C(5)) bonds. The latter "long" bond distances are longer than what one would expect for a typical η^4 coordination.[13] Both **C-Fe** and **D-Fe** intermediates are 16-electron species and therefore are less stable than their 18-electron isomers **A-Fe** and **B-Fe**. Their electron deficiency is associated with a metal-centered LUMO lying at a rather low

(12) Calhorda, M. J.; Goncalves, I. S.; Herdtweck, E.; Romão, C. C.; Royo, B.; Veiros, L. F. *Organometallics* **1999**, *18*, 3956.

(13) Gonzálvez-Blanco, O.; Branchadell, V. *Organometallics* **1997**, *16*, 475.

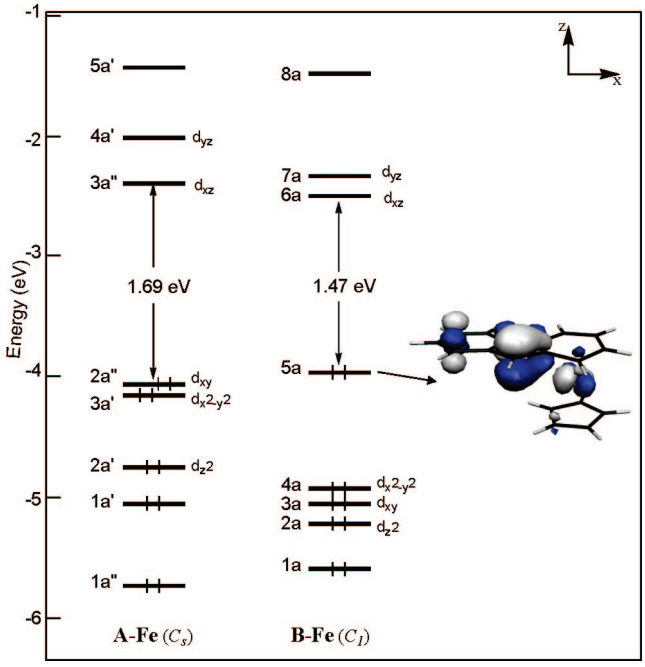

Figure 4. MO level ordering of **A-Fe** and **B-Fe** (BP86 calculations).

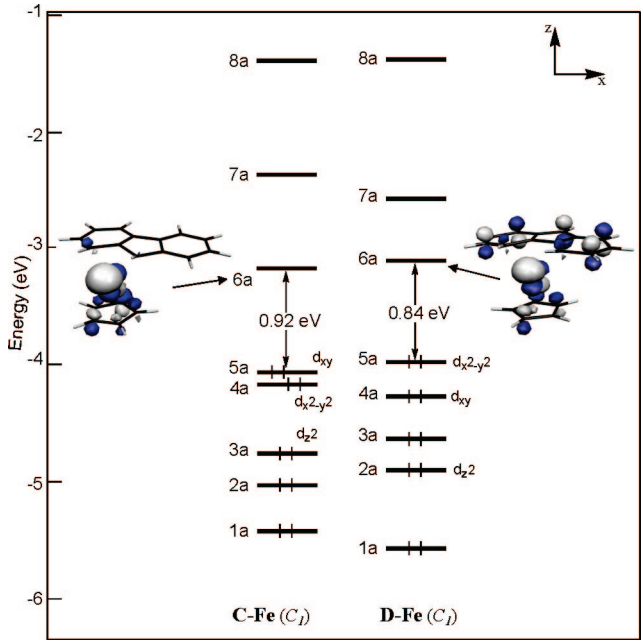

Figure 5. MO level ordering of **C-Fe** and **D-Fe** (BP86 calculations).

energy, as shown by their MO level ordering shown in Figure 5 (BP86 level). The topology of these orbitals (see Figure 5) provides **C-Fe** and **D-Fe** with potential bonding ability to incoming Lewis bases. Thus, the use of solvents with significant coordinating capability should modify the energetics of the observed HRR. The fact that **C-Fe** was found more stable than **D-Fe** by several kcal·mol^{-1} at both levels of calculations is related to their different modes of coordination to the Flu^{-} ligand. In **D-Fe**, the ligand donates two π(C═C) bonding electron pairs to the metal. In **C-Fe**, it donates formally one π(C═C) pair and one π lone pair, the latter being much more available for bonding to the metal.

Four transition states associated with HRR between **A-Fe** and **B-Fe** via the two possible low-coordinate intermediates **C-Fe** and **D-Fe** were then located. The corresponding energy profiles are sketched in Figure 6. Both transition states involving the **C-Fe** intermediate, namely, $\mathbf{TS_{A\rightarrow C}}$ and $\mathbf{TS_{C\rightarrow B}}$, feature an exocyclic η^2 coordination of the fluorenyl ligand and noncoplanar orientation of the Cp and Flu planes (Table 3 and Figure 3). Similarly, the transition states mediating the alternative "backside" pathway ($\mathbf{TS_{A\rightarrow D}}$ and $\mathbf{TS_{D\rightarrow B}}$) reveal reduced coordination of the fluorenyl moiety with the iron center, i.e., η^2 and η^3, respectively. $\mathbf{TS_{C\rightarrow B}}$ is 5.3 kcal·mol^{-1} at the B3LYP level (4.3 kcal·mol^{-1} with the BP86 functional) lower in energy than the alternative $\mathbf{TS_{D\rightarrow B}}$ intermediate for the "backside" trajectory (see Figure 6). This energy difference reflects at least for a part that of the **C-Fe** and **D-F** intermediates. Thus, calculations indicate that the most favored HRR between **A-Fe** and **B-Fe** occurs through the **C-Fe** intermediate. It turns out that the corresponding computed activation barrier for the **B-Fe** ⇆ **A-Fe** HRR ($\Delta E^{\ddagger}_{B\rightarrow A}$ = 27.3 (33.2) kcal·mol^{-1}) is very close to the one measured experimentally for this system ($\Delta E^{\ddagger}_{B\rightarrow A}$ = 31.4 ± 2.2. kcal·mol^{-1}, vide supra).

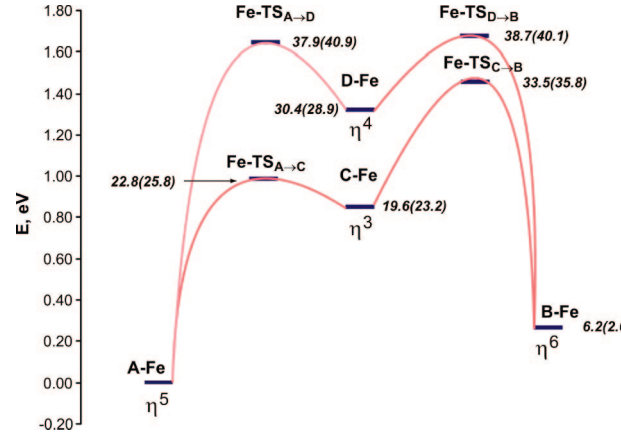

Figure 6. Calculated energy profile for [(Cp)Fe(η^6-Flu)] (**B-Fe**) ⇆ [(Cp)Fe(η^5-Flu)] (**A-Fe**) process at the B3LYP(BP86)/LANL2DZ(f) level. Energy differences (in italics) are given in kcal·mol^{-1} relative to **A-Fe**.

(Cp)Ru(η^n-Flu). Owing to the similarities between the data computed with the B3LYP and BP86 functionals in the case of (Cp)Fe(η^n-Flu), the analogous ruthenium system was investigated only at the B3LYP level, which is expected to provide more accurate energetics. The major data are summarized in Table 4. Similarly to the iron case, **A-Ru** was found a few kcal·mol^{-1} more stable than **B-Ru** and the optimized geometry of **A-Ru** agrees well with the experimental structure.[6] As in the iron system, two intermediates, **C-Ru** and **D-Ru**, with identical structures to their Fe counterparts were identified. Also, the **C-Ru** intermediate was found to be more stable than the **D-Ru** intermediate. The transition states linking the four minima (not shown here) were also found to have similar geometries and electronic structures to their iron homologues. As a result, the energy profile of the Ru system, shown in Figure 7, is very similar to that of the Fe system (Figure 6). Consequently, the favored **A-Ru** ⇆ **B-Ru** HRR is predicted to occur through the **C-Ru** intermediate with a computed activation barrier of 32.4 kcal·mol^{-1}. Although this barrier is somewhat higher than that found for the iron system, it should allow the observation of the **A-Ru** ⇆ **B-Ru** HRR at reasonable temperatures. Moreover, the small computed energy difference between the isomers (4.5 kcal·mol^{-1}) suggests that the isolation of **B-Ru**, (C_5Me_5)Ru(η^6-Flu), is plausible.

Table 4. Major Computed Data for the HRR Process A-Ru ⇆ B-Ru (B3LYP level) (values in square brackets are average experimental values for A-Ru (ref 6))

	A-Ru	B-Ru	C-Ru	D-Ru	$TS_{A\rightarrow C}$	$TS_{C\rightarrow B}$	$TS_{A\rightarrow D}$	$TS_{D\rightarrow B}$
HOMO–LUMO gap (eV)	3.67	3.16	3.02	2.20	2.99	2.15	1.90	2.28
rel energy (kcal·mol^{-1})	0	4.5	17.3	27.3	21.3	32.4	38.5	35.2
Ru−C(1) (Å)		2.340	2.438		2.586	2.256		
Ru−C(2) (Å)		2.263						
Ru−C(3) (Å)		2.247						
Ru−C(4) (Å)		2.283		2.543			2.591	2.289
Ru−C(5) (Å)				2.543				
Ru−C(10) (Å)	2.317 [2.227(5)]	2.599	2.292		2.342	2.342	3.086	3.142
Ru−C(11) (Å)	2.336 [2.226(5)]	2.380	3.242	2.295	3.194	3.120	2.388	2.306
Ru−C(12) (Å)	2.336 [2.243(5)]			2.295			2.316	
Ru−C(13) (Å)	2.317 [2.227(5)]							
Ru−C(9) (Å)	2.230 [2.183(6)]		2.212		2.235	2.881		
Ru−C(Cp) (Å) average	2.235 [2.156]	2.247	2.214	2.205	2.198	2.204	2.194	2.186
Ru−C(Cp) (Å) range	2.224–2.247 [2.143–2.169]	2.245–2.249	2.155–2.283	2.172–2.253	2.141–2.248	2.164–2.261	2.135–2.244	2.163–2.224
dipole moment μ (D)	0.54	4.33	1.90	2.41	3.48	2.09	3.34	3.68

Conclusion

The dynamic phenomenon in (Cp)Fe(η^n-Flu) associated with the haptotropic $\eta^6 \leftrightarrows \eta^5$ metal migration process was investigated by NMR spectroscopy. In agreement with the preceding studies on this system,[2] the reaction was characterized as a first-order reversible process with activation parameters $\Delta E^{\ddagger}_{B\rightarrow A}$ of 31.4 ± 2.2 kcal·mol^{-1} and $\Delta S^{\ddagger}_{B\rightarrow A}$ of 24 ± 5 eu. Very similar energy barrier values were obtained from DFT calculations using both B3LYP and BP86 functionals, i.e., 27.3 and 33.2 kcal·mol^{-1}, respectively. The theoretical study disclaims least-motion pathways between two adjacent rings of the fluorenyl moiety in (Cp)Fe(η^n-Flu) and rather suggests an alternative indirect trajectory via the front- and/or backsides of the π-framework mediated by two low-coordinate intermediates **C-Fe** ("frontside" asymmetric η^3-allylic-like complex) and **D-Fe** ("backside" symmetric η^4-butadienic-like complex). The former pathway appears to be preferred over the latter one, considering that **C-Fe** is 5–10 kcal/mol more stable than **D-Fe**, and that it is attainable through a lower energy (4–5 kcal·mol^{-1}) transition state. Application of this theoretical model to the (Cp)Ru(η^n-Flu) system led to the location of intermediates and transition states of similar geometry and comparable energy profile to those in the iron case. These computations suggest that (i) the **A-Ru** ⇆ **B-Ru** haptotropic rearrangement process could be achieved at reasonable temperatures, and (ii) **B-Ru**, (C_5Me_5)Ru(η^6-Flu), could be experimentally isolated as well, likely via deprotonation of a pre-η^6-coordinated fluorene intermediate $[(C_5Me_5)Ru(\eta^6\text{-FluH})]^+$, as we did in the present study for iron.

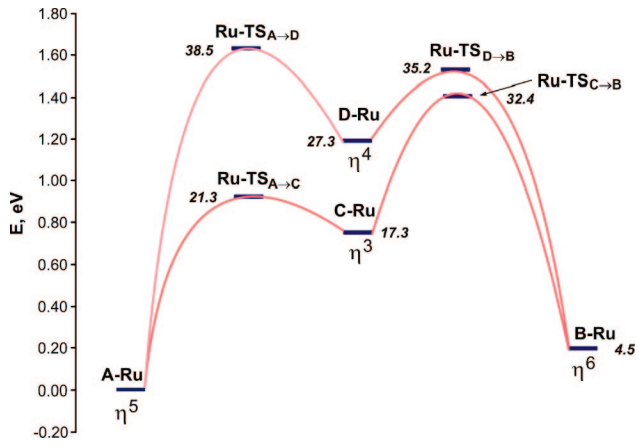

Figure 7. Calculated energy profile for the [(Cp)Ru(η^6-Flu)] (**B-Ru**) ⇆ [(Cp)Ru(η^5-Flu)] (**A-Ru**) process at the B3LYP/LANL2DZ(f) level. Energy differences (in italics) are given in kcal·mol^{-1} relative to **A-Ru**.

Experimental Section

General Considerations. All manipulations were performed under a purified argon atmosphere using standard Schlenk techniques or in a glovebox. Toluene was distilled from Na/K alloy under argon, degassed thoroughly, and stored under argon prior to use. Deuterated solvents (benzene-d_6, toluene-d_8, cyclohexane-d_{12}; >99.5% D, Eurisotop) were vacuum-transferred from Na/K alloy into storage tubes. Complex [(Cp)Fe(η^6-Flu)] (**B-Fe**) was prepared from commercially available [(Cp)Fe(η^6-FluH)]PF_6 (Aldrich) using the reported procedure.[1e] NMR spectra of complexes were recorded on a Bruker AM-500 spectrometer in Teflon-valved NMR tubes. ^{1}H chemical shifts are reported in ppm vs $SiMe_4$ and were determined by reference to the residual solvent peaks.

Kinetic Investigations. Monitoring by ^{1}H NMR Spectroscopy. In the glovebox, a solution of [(Cp)Fe(η^6-Flu)] (**B-Fe**) (30–35 μmol in ca. 0.5 mL of benzene-d_6 or cyclohexane-d_{12}) was transferred into an NMR tube equipped with a J. Young stopcock. NMR spectra were recorded regularly after a certain time period at the required temperature using the Bruker software suite embedded procedure. The kinetic data were processed using the equation of the first-order reversible reaction:

$$\ln\frac{X_{eq}}{X_{eq}-X_t} = (k + 2k_{-1})t$$

where k and k_{-1} are the rate constants of the "forward" and "backward" reactions, respectively; X_{eq} and X_t are the molar concentrations of complex **B** in the equilibrium state and at the moment t, respectively.[2]

The activation parameters for the HRR process were obtained from a standard least-squares Eyring analysis according to the equation

$$\ln\left(\frac{k}{T}\right) = -\frac{\Delta E^{\#}}{RT} + \frac{\Delta S^{\#}}{R} + \ln\frac{k_B}{h}$$

where k is the first-order rate constant and k_B is the Boltzmann constant. The standard deviations from the least-squares fit were used to estimate the uncertainties in $\Delta E^{\ddagger}$ and $\Delta S^{\ddagger}$.[14]

(14) (a) Bevington, P. R. *Data Reduction and Error Analysis for the Physical Sciences*; McGraw-Hill: New York, 1969. (b) Skoog, D. A.; Leary, J. J. *Principles of Instrumental Analysis*, 4th ed.; Saunders College: Fort Worth, TX, 1992; pp 13–14.

(15) Altomare, A.; Burla, M. C.; Camalli, M.; Cascarano, G.; Giacovazzo, C.; Guagliardi, A.; Moliterni, A. G. G.; Polidori, G.; Spagna, R. *J. Appl. Crystallogr.* **1999**, *32*, 115.

Solid State Structure Determination of Complex A-Fe. A suitable single crystal of **A-Fe** was mounted onto a glass fiber using the "oil-drop" method. Diffraction data were collected at 100 K using an APEXII Bruker-AXS diffractometer with graphite-monochromatized Mo Kα radiation ($\lambda = 0.71073$ Å). A combination of ω- and φ-scans was carried out to obtain at least a unique data set. The structure was solved by direct methods using the SIR97 program[15] and then refined with full-matrix least-squares methods based on F^2 (SHELX-97)[16] with the aid of the WINGX[17] program. Many hydrogen atoms could be found from the Fourier difference. Carbon-bound hydrogen atoms were placed at calculated positions and forced to ride on the attached carbon atom. The hydrogen atom contributions were calculated but not refined. All non-hydrogen atoms were refined with anisotropic displacement parameters. The locations of the largest peaks in the final difference Fourier map calculation as well as the magnitude of the residual electron densities were of no chemical significance. Main crystallographic data are available as Supporting Information, as a cif file.

Computational Details. DFT calculations were carried out using the Gaussian 03 package,[18] employing B3LYP[19] and/or BP86[20] functionals (see text), and using a standard double-ξ polarized basis set, namely the LANL2DZ set, augmented with a single polarization f function on iron and ruthenium (of exponent 0.8 and 0.4, respectively). The C_s symmetry constraint was applied on **A-Fe** and **A-Ru**. All stationary points were fully characterized via analytical frequency calculations as either true mimina (all positive eigenvalues) or transition states (one imaginary eigenvalue). The IRC procedure was used to confirm the nature of each transition state connecting two minima. Zero-point vibrational energy corrections (ZPVE) were estimated by a frequency calculation at the same level of theory, to be considered for the calculation of the total energy values. Molecular orbital plots were generated using the program MOLEKEL 4.3.[21]

Acknowledgment. Calculations were carried out at the French national computing centers IDRIS (CNRS-Orsay) and CINES (Montpellier). J.-Y.S. and J.-F.C. thank the Institut Universitaire de France (IUF) for support of this research.

Supporting Information Available: Additional data on the processing of kinetic data and the crystal structure determination of **A-Fe**, also as a cif file; tables of Cartesian coordinates and energies of all the computed stationary points. This material is available via the Internet at http://pubs.acs.org.

OM701109Z

(16) (a) Sheldrick, G. M. *SHELXS-97*, Program for the Determination of Crystal Structures; University of Goettingen: Germany, 1997. (b) Sheldrick, G. M. *SHELXL-97*, Program for the Refinement of Crystal Structures; University of Goettingen: Germany, 1997.

(17) Farrugia, L. J. *J. Appl. Crystallogr.* **1999**, *32*, 837.

(18) Frisch, M. J.; Trucks, G. W.; Schlegel, H. B.; Scuseria, G. E.; Robb, M. A.; Cheeseman, J. R.; Montgomery, J. A.; Vreven,T., Jr.; Kudin, K. N.; Burant, J. C.; Millam, J. M.; Iyengar, S. S.; Tomasi, J.; Barone, V.; Mennucci, B.; Cossi, M.; Scalmani, G.; Rega, N.; Petersson, G. A.; Nakatsuji, H.; Hada, M.; Ehara, M.; Toyota, K.; Fukuda, R.; Hasegawa, J.; Ishida, M.; Nakajima, T.; Honda, Y.; Kitao, O.; Nakai, H.; Klene, M.; Li, X.; Knox, J. E.; Hratchian, H. P.; Cross, J. B.; Adamo, C.; Jaramillo, J.; Gomperts, R.; Stratmann, R. E.; Yazyev, O.; Austin, A. J.; Cammi, R.; Pomelli, C.; Ochterski, J. W.; Ayala, P. Y.; Morokuma, K.; Voth, G. A.; Salvador, P.; Dannenberg, J. J.; Zakrzewski, V. G.; Dapprich, S.; Daniels, A. D.; Strain, M. C.; Farkas, O.; Malick, D. K.; Rabuck, A. D.; Raghavachari, K.; Foresman, J. B.; Ortiz, J. V.; Cui, Q. ; Baboul, A. G.; Clifford, S.; Cioslowski, J.; Stefanov, B. B.; Liu, G.; Liashenko, A.; Piskorz, P.; Komaromi, I.; Martin, R. L.; Fox, D. J.; Keith, T.; Al-Laham, M. A.; Peng, C. Y.; Nanayakkara, A.; Challacombe, M.; Gill, P. M. W.; Johnson, B.; Chen, W.; Wong, M. W.; Gonzalez, C.; Pople, J. A. *Gaussian 03, Revision B.04*; Gaussian, Inc.: Pittsburgh, PA, 2003.

(19) (a) Becke, A. D. *Phys. Rev. A* **1988**, *38*, 3098. (b) Becke, A. D. *J. Chem. Phys.* **1993**, *98*, 5648. (c) Lee, C.; Yang, W.; Parr, R. G. *Phys. Rev. B* **1988**, *37*, 785.

(20) Perdew, J. P. *Phys. Rev. B* **1986**, *33*, 8822.

(21) Flukiger, P.; Luthi, H. P.; Portmann, S.; Weber, J. *MOLEKEL 4.3*; Swiss Center for Scientific Computing: Manno, Switzerland, 2000; http://www.cscs.ch.